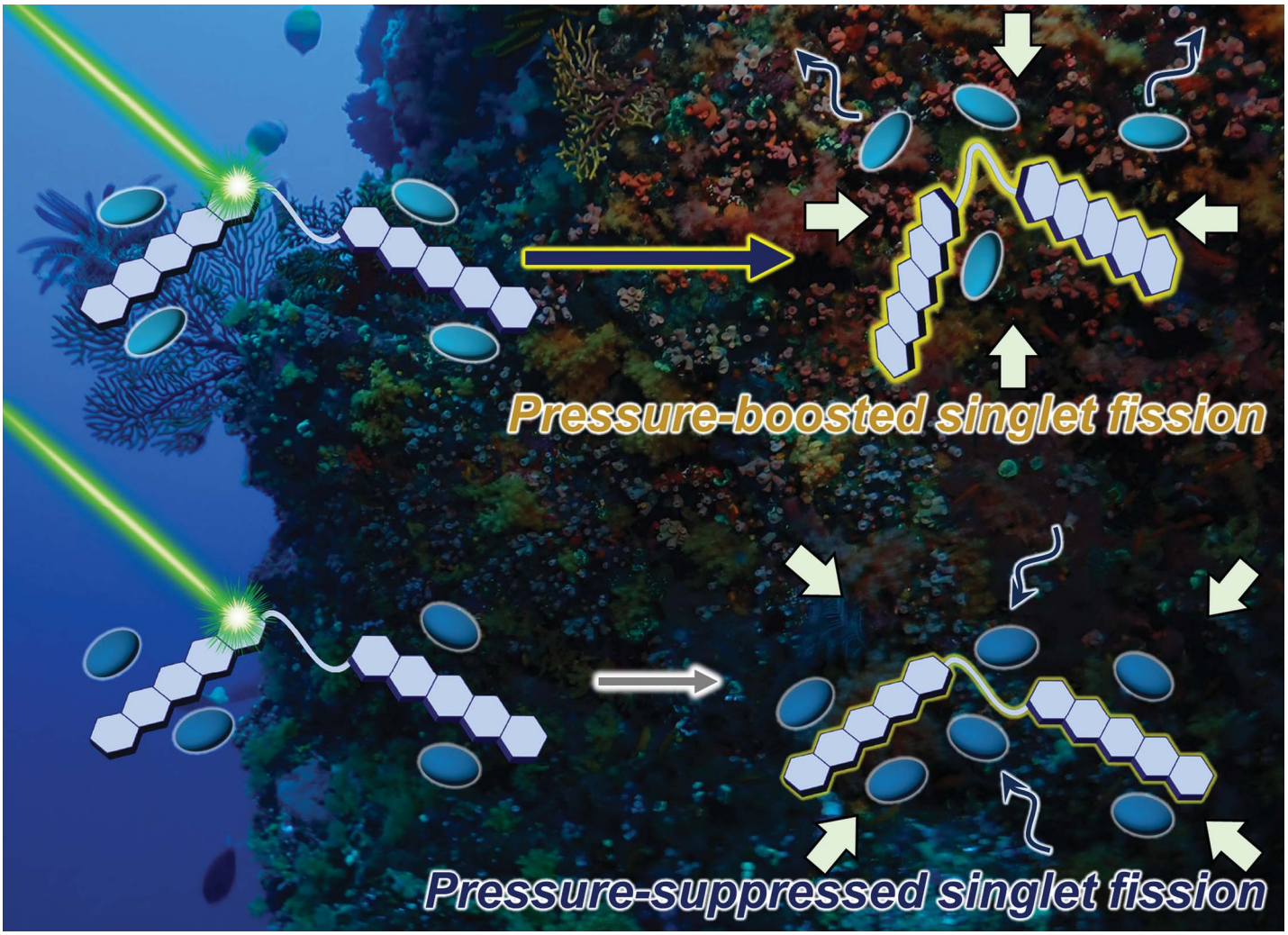

Showcasing research from the laboratories of Professor Fukuhara, Institute for Materials Chemistry and Engineering, Kyushu University, Japan.

Critical molecular design that can actively control intramolecular singlet fission by hydrostatic pressure

In this study, we revealed how and to what extent hydrostatic pressure stimulation affects the singlet fission process by using novel singlet fission materials with flexible linkers. The highlighted results obtained here were the dynamic control of intramolecular singlet fission kinetics and T_1 formation thermodynamics, both of which were achievable *via* this *critical molecular design.*

Image reproduced by permission of Gaku Fukuhara from *Chem. Sci.,* 2025, **16**, 20245.

As featured in:

See Taku Hasobe, Gaku Fukuhara *et al.,* *Chem. Sci.,* 2025, **16**, 20245.

ROYAL SOCIETY OF CHEMISTRY

15 YEARS ANNIVERSARY

rsc.li/chemical-science

Registered charity number: 207890

Chemical Science

ROYAL SOCIETY OF CHEMISTRY

EDGE ARTICLE

View Article Online
View Journal | View Issue

Cite this: *Chem. Sci.*, 2025, **16**, 20245

All publication charges for this article have been paid for by the Royal Society of Chemistry

Critical molecular design that can actively control intramolecular singlet fission by hydrostatic pressure

Rintaro Ogawa,[a] Tomokazu Kinoshita,[a] Tomoya Kuwabara,[a] Hayato Sakai,[b] Makoto Harada,[a] Taku Hasobe *[b] and Gaku Fukuhara *[ac]

Received 29th June 2025
Accepted 10th October 2025

DOI: 10.1039/d5sc04791a

rsc.li/chemical-science

The active control of singlet fission (SF) by external stimuli presents a major challenge in current chemistry, although it is yet in the initial stages. In this study, we synthesized a series of SF-active chromophore pentacene dimers connected by the flexible linkers and investigated the ground- and excited-state properties, under hydrostatic pressure as an external stimulus. The flexibilities of the linkers were elucidated by the density functional theory. Hydrostatic pressure-UV/vis and hydrostatic pressure-circular dichroism spectroscopies showed the absence of a ground-state conformational change, indicating that the active switching of SF observed in this study comes from the excited-state dynamics. The hydrostatic pressure-fluorescence lifetime and hydrostatic pressure-nanosecond transient absorption measurements revealed the active inversion of SF process (acceleration *vs.* deceleration) and independent triplet (T_1) formation, in addition to the shortened T_1 lifetimes and non-decreasing T_1 quantum yields with elevating hydrostatic pressure. This study offers a valuable guideline through the critical molecular design revealed herein for further developing smart SF-controllable soft materials induced by hydrostatic pressure stimulations.

Introduction

The development of up-converting reactions in terms of energy and yield is a long-term dream for scientists. Such an up-hill type of reaction is capable of being constructed in photochemistry. For instance, upconversion[1–3] and singlet fission (SF)[4–6] are well-known photophysical processes, and the latter has attracted considerable attention recently. SF is a process where an excited chromophore (S_1 exciton) interacts with a ground-state one (S_0) resulting in correlated triplet pairs (^{1}TT and ^{5}TT)[7,8] subsequently relaxing to two individual T_1 excitons (Fig. 1a (top)). Such promising SF systems, particularly in solution state are still in their infancy and have been actively pursued since the first observation of the correlated ^{1}TT in 2013.[7] The importance of the solution-state SF systems has gradually increased[9–11] owing to a better possibility as a highly efficient triplet photosensitizer through excited triplet photoreactions,[12] such as the formation of singlet oxygen,[13] which can be utilized in photodynamic therapy (PDT) toward cancer treatment.[14,15] Therefore, the construction of a large variety of SF-based functional materials is essential, although a major challenge in current chemistry.

Nevertheless, the development of a multifarious molecular design that is rich in variety is hampered by a limitation from an energy standpoint: the energy balance at the excited singlet and triplet levels in each chromophore acquires the relationship as $E(S_1) \geq 2E(T_1)$.[4–6] Acenes, such as tetracene and pentacene (Pc), have become the first choice as the chromophore for SF, as they strictly satisfy such an energy balance.[16,17] In other words, modifying the chromophores are not suitable when aiming toward a high efficiency of SF materials. Accordingly, the mainstream trend is recently seen shifting to an active control of SF properties by external stimuli such as temperature,[18–21] solvent,[22–24] supramolecular complexation,[24–28] and mechanical forces.[29–32] In particular, a pressure stimulation as an active means of control seems to be compatible with the triplet-state PDT reaction in biological systems, as the current mechanobiology has revealed that the fate of cells can be determined by the mechanical pressure.[33,34]

Hydrostatic pressure, an isotropic mechanical force, is a unique and ubiquitous stimulation that plays significant roles in controlling chemical, physical, and the abovementioned biological events.[34–37] Since the beginning of the 1960s,[38] the hydrostatic pressure effects on photophysical and photochemical processes, such as excimer/exciplex,[39,40] photoinduced electron transfer,[41] twisted intramolecular charge transfer,[42] photocycloaddition,[43,44] and so on, have been extensively

[a]*Department of Chemistry, Institute of Science Tokyo, 2-12-1 Ookayama, Meguro-ku, Tokyo 152-8551, Japan*

[b]*Department of Chemistry, Faculty of Science and Technology, Keio University, Yokohama, Kanagawa 223-8522, Japan. E-mail: hasobe@chem.keio.ac.jp*

[c]*Institute for Materials Chemistry and Engineering, Kyushu University, 744 Motooka, Nishi-ku, Fukuoka 819-0395, Japan. E-mail: gaku@ms.ifoc.kyushu-u.ac.jp*

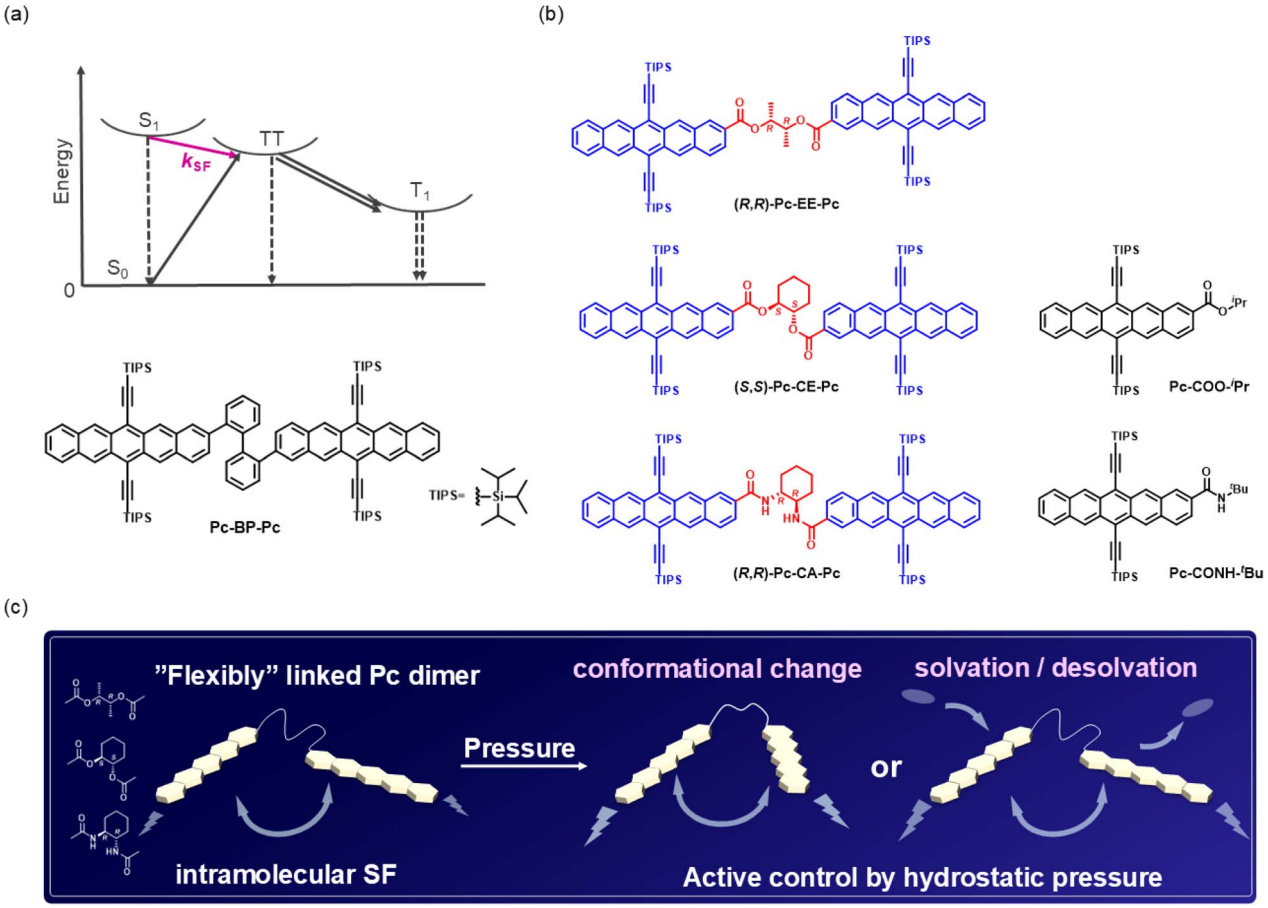

Fig. 1 (a) (Top) schematic diagram of SF in a TIPS-modified pentacene (Pc) dimer: k_{SF} represents the rate constant of SF from S_1 to TT; in the present Pc case, the reverse triplet–triplet annihilation (TTA) can be omitted, due to the large exergonic reaction (*ca.* 0.3 eV).[45] (Bottom) chemical structure of **Pc-BP-Pc**. (b) Chemical structures of SF-active dimers; **(*R*,*R*)-Pc-EE-Pc**, **(*S*,*S*)-Pc-CE-Pc**, and **(*R*,*R*)-Pc-CA-Pc**, the corresponding referenced monomers; **Pc-COO-^{i}Pr** and **Pc-CONH-^{t}Bu**. (c) Conceptual illustration of active control of SF-active soft materials driven by hydrostatic pressure.

investigated. However, the "young" SF field has just begun, with our recent work published in 2023 as the first example.[31] For that reason, the molecular design of the targeted SF material for the active control stimulated by hydrostatic pressure was still performed on a trial-and-error basis. Meanwhile, previous research[31] offers a reasonable guideline where connecting each acene by a more "active" and "flexible" linker appears to be better rather than by the use of the relatively "rigid" scaffold; accordingly, a biphenyl linker was employed in **Pc-BP-Pc**, as shown in Fig. 1a (bottom).

In this study, to investigate how and to what extent the hydrostatic pressure stimulation affects the SF process, we designed novel SF materials (**(*R*,*R*)-Pc-EE-Pc**, **(*S*,*S*)-Pc-CE-Pc**, and **(*R*,*R*)-Pc-CA-Pc**, as shown in colors in Fig. 1b (left)), where the SF-chromophoric pentacenes were connected with relatively flexible cyclohexanes and the more flexible alkane, and also arranged the corresponding referenced monomers (**Pc-COO-^{i}Pr** and **Pc-CONH-^{t}Bu**, shown in black in Fig. 1b (right)) for the sake of comparison. The comprehensive study will reveal the critical factors that govern the SF dynamics induced by hydrostatic pressure, as illustrated in Fig. 1c. Herein, we report an unprecedented SF dynamics inversion (acceleration *vs.* deceleration) driven by a good combination of hydrostatic pressure and solvation stimulations. The results obtained and concepts proposed herein will enable us to construct actively controllable SF materials based on the established molecular design guidelines.

Results and discussion

Activity in SF materials

In the active control of SF by hydrostatic pressure, the rotational freedom of the linkers connecting pentacenes plays a decisive role. Therefore, to confirm the linker flexibility in the target SF materials, quantum chemistry calculations by density functional theory (DFT) were performed on the model linkers (**BP**, **Cy**, and **Et**). As shown in Fig. 2, the energy–dihedral angle diagram indicates that the **Cy** linker can rotate at a lower energy as 55 kJ than **BP** as 69 and 88 kJ. Furthermore, the **Et** alkane chain has a low energy of 28 kJ, which is less than half of that corresponding to **BP**. Therefore, the calculation results concluded the order of the rotational barrier in the linkers as **BP**

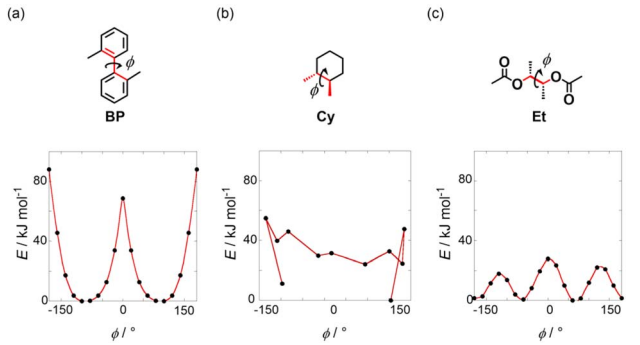

Fig. 2 Potential energy landscape as a function of dihedral angles of (a) **BP**, (b) **Cy** (data were extracted from ref. 46 for the plot), and (c) **Et**, calculated at ωB97xd/6-31G(d,p). The most stable conformers in each linker were set at 0 kJ mol^{-1}. The sudden hysteresis jump in (b) was due to the ring flip.

> **Cy** > **Et**, which indicates that the present SF materials (**Pc-CA-Pc**, **Pc-CE-Pc**, and **Pc-EE-Pc**) may be more susceptible to hydrostatic pressure compared with the previous **Pc-BP-Pc**.

Hydrostatic pressure-spectral experiments in SF materials

In the hydrostatic pressurized conditions, it is first required to confirm whether the SF materials behave as a monomeric state even at the pressure conditions of up to 160 MPa, the highest tested in this study. Thus, we investigated **Pc-CA-Pc**, **Pc-CE-Pc**, and **Pc-EE-Pc** in toluene and methylcyclohexane (MCH) as a good and poor solvent at 0.1 and 160 MPa. Fig. 3 shows the results corresponding to **Pc-EE-Pc**. The normalized UV/vis absorption spectra (middle panels in Fig. 3) were completely matched with each other in the concentration range of 13–401 μM without any spectral changes. Additionally, the standard linear curves as a function of concentration gave good straight lines under both pressures. These results indicate that the pressure-induced aggregation and crystallization of **Pc-EE-Pc** do not proceed in this concentration range, which means that the following hydrostatic pressure experiments enable us to treat the SF materials as a monomeric state, that is "intramolecular" SF (iSF) process. Other concentration-dependent results are also given in Fig. S2–S5 in SI. The only exception was the condition of an MCH solution of **Pc-CA-Pc**, shown in Fig. S6. The normalized UV/vis absorption spectra showed a slight bathochromic shift with increasing concentration under both pressures, indicating an intermolecular J-type aggregation[47] due to the amide bond possessing a hydrogen-bonding ability. Hence, the subsequent hydrostatic pressure experiments of **Pc-CA-Pc** were performed only in toluene.

Next, we investigated by means of hydrostatic pressure-UV/vis and hydrostatic pressure-circular dichroism (CD) spectra to determine whether a ground-state conformational change of the SF materials (Pc dimers) is induced by hydrostatic pressure. As a control experiment, we used **Pc-COO-^{i}Pr** and **Pc-CONH-^{t}Bu** as the corresponding referenced monomers that are considered to behave as each monomer without SF, and compared with data obtained from the Pc dimers. As shown in Fig. 4 (top), S7 and S8, toluene solutions of the three Pc dimers and two monomers showed the monotonic hyperchromic effects and the stepwise bathochromic shifts in the hydrostatic pressure-UV/vis absorption spectra. The former simply comes from the increasing of the effective concentration due to the compression. The latter originates from changes in solvent density/polarizability induced by hydrostatic pressure,[38] the degree of which enables us to elucidate the hydrostatic pressure effects. In Fig. S7–S15, all the data were summarized. Also, the other

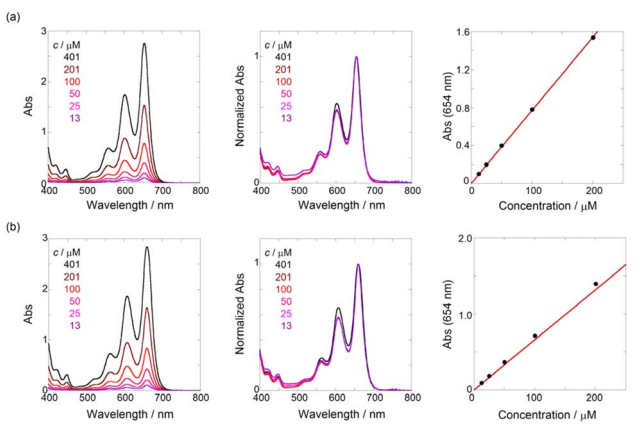

Fig. 3 Concentration-dependent (13–401 μM) UV/vis spectra (left), normalized UV/vis spectra (middle), and absorbance plots (13–201 μM) (right) of **Pc-EE-Pc** in toluene at (a) 0.1 MPa (correlation coefficient r = 1.000, slope = 0.0077 (±3.9 × 10^{-5}) μM^{-1}) and (b) 160 MPa (r = 0.999, slope = 0.0064 (±0.00013) μM^{-1}) at room temperature, measured in a high-pressure cell.

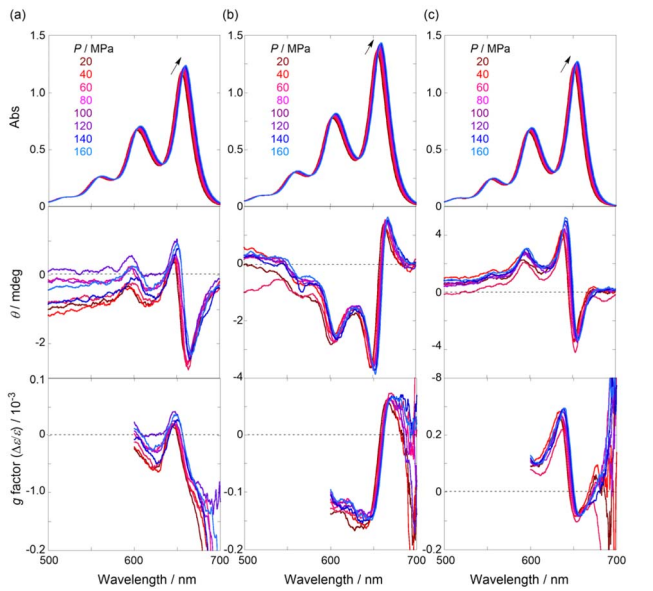

Fig. 4 Pressure-dependent UV/vis absorption (top), CD (middle), and anisotropy (g) factor (=Δε/ε) (bottom) spectra of (a) (*R*,*R*)-**Pc-EE-Pc** (144 μM), (b) (*S*,*S*)-**Pc-CE-Pc** (142 μM), and (c) (*R*,*R*)-**Pc-CA-Pc** (136 μM) in toluene at room temperature at 20, 40, 60, 80, 100, 120, 140, and 160 MPa, measured in a high-pressure cell. The g factor profiles <600 nm were omitted due to the baseline noises.

important fact is that the spectra at 0.1 MPa depressurized from 160 MPa (green lines) were superimposable with the original spectra at 0.1 MPa (black lines), which indicates that the present pressurization cycle was completely reversible. Further, as summarized in Table S1, the Pc dimers exhibited the pressure-induced red shifts of −0.841 to −0.925 cm^{-1} MPa^{-1} in toluene and −0.798 to −0.810 cm^{-1} MPa^{-1} in MCH, whereas the monomers showed those of −0.913 to −0.925 cm^{-1} MPa^{-1} in toluene and −0.804 cm^{-1} MPa^{-1} in MCH, indicating good agreement with the shift values of dimers and monomers. Also, other π-conjugated systems, *e.g.*, anthracene, pyrene, and perylene, generally showed approximately −1 cm^{-1} MPa^{-1}.[37,48–50] The pressure-induced red shifts are likely to be responsible for the data based on the absence of specific ground-state conformational change of the Pc dimers. More importantly, as a better molecular design, chiralities are incorporated into the present Pc dimers, which enables us to more precisely elucidate the conformational changes by using the hydrostatic pressure-CD spectroscopy. As shown in Fig. 4 (middle and bottom), the CD and corresponding anisotropy (*g*) factor profiles showed clear bisignate couplings at the longer wavelengths. According to the exciton chirality theory,[51] **(*R*,*R*)-Pc-EE-Pc** and **(*R*,*R*)-Pc-CA-Pc** showed the negative exciton coupling, whereas **(*S*,*S*)-Pc-CE-Pc** gave the positive one. The most important realization is the fact that the amplitudes of all the Pc dimers in *g* factor do not change with elevating pressure despite of slight red shifts in UV/vis, clearly revealing the absence in ground-state conformational changes around the flexible linkers. Hence, it should be noted that the below-mentioned active SF properties induced by hydrostatic pressure comes from not ground-state equilibria but excited-state kinetics.

iSF processes in toluene under 0.1 MPa and hydrostatic pressures

The results of the negligible ground-state conformational changes allowed us to further estimate the iSF kinetics of the Pc dimers under hydrostatic pressures. First, to confirm the SF process of such active-linked Pc dimers at an ambient pressure (0.1 MPa), we compared the fluorescence lifetimes of the Pc dimers with those of the monomers in toluene. As shown in Fig. 5, the dimers' profiles revealed fast decays rather than those of the references, clearly indicating the faster quenching in the dimer skeletons, that is SF process. Hence, we decided to elucidate the apparent rate constant of SF ($k_{SF,app}$) based on data obtained from fluorescence lifetime decays, as was the case with the previous report as **Pc-BP-Pc**.[31] Note that: it is merely an apparent value calculated based on the following process. That is, the meaning of $k_{SF,app}$ is that for convenience of analysis, the τ_1 component of the reference monomer is used instead of the τ_2 component of the dimer, which is more susceptible to some fluctuations. In the case of **Pc-BP-Pc**, $k_{SF,app}$ for the generation of the TT can be written as eqn (1):

$$k_{SF,app} = (k_{SF} + k_0) - k_0 = \frac{1}{\tau_{1,\,dimer}} - \frac{1}{\tau_{1,\,ref}} \quad (1)$$

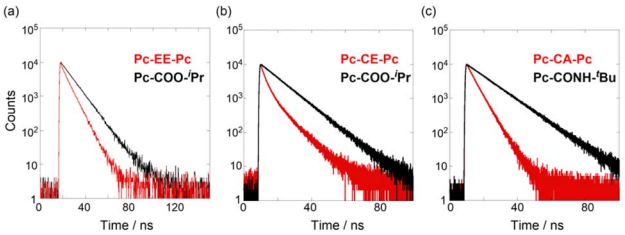

Fig. 5 Time-correlated fluorescence decays (λ_{ex} 590 nm) of (a) **Pc-EE-PC** (44 μM, λ_{obs} 665 nm; red) and **Pc-COO-^{i}Pr** (82 μM, λ_{obs} 665 nm; black), (b) **Pc-CE-Pc** (41 μM, λ_{obs} 665 nm; red) and **Pc-COO-^{i}Pr** (82 μM, λ_{obs} 665 nm; black), and (c) **Pc-CA-Pc** (41 μM, λ_{obs} 660 nm; red) and **Pc-CONH-^{t}Bu** (89 μM, λ_{obs} 656 nm; black) in toluene at room temperature at 0.1 MPa, measured in a high-pressure cell.

where k_0 represents the decay rate constant from the singlet excited-stated reference monomer, which can be estimated as a reciprocal of the reference fluorescence lifetime. In contrast, the term of (k_{SF} + k_0) can be elucidated as a reciprocal of the dimer fluorescence lifetime. **Pc-BP-Pc** has two fluorescence lifetime species as τ_1 and τ_2 in which long-lived τ_2 is ascribed as the fluorescence emission from the S_1 pentacene monomer without SF and thus short-lived τ_1 involved the SF decay.[31,52] Namely, the $\tau_{1,ref}$ species emits the fluorescence as a monomer (without the SF process) and the $\tau_{1,dimer}$ species mainly decays as a deactivation path (involved the SF process). In fact, as summarized in Tables 1 and S2–S12, and Fig. S16–S26, the

Table 1 Fluorescence lifetimes and apparent rate constants of singlet fission ($k_{SF,app}$) of all the compounds in toluene at 0.1 MPa[a]

Compd	τ_1/ns	A_1	τ_2/ns	A_2	χ^2	$k_{SF,app}/10^8$ s^{-1}
Pc-EE-Pc (44 μM)	1.3	0.07	6.6	0.93	1.16	6.84
Pc-CE-Pc (41 μM)	2.4	0.54	8.3	0.46	1.22	3.33
Pc-CA-Pc (41 μM)	3.0	0.21	5.3	0.79	1.24	2.54
Pc-COO-^{i}Pr (82 μM)	10.9	1.00			1.16	[b]
Pc-CONH-^{t}Bu (89 μM)	12.5	1.00			1.00	[b]

[a] Fluorescence lifetime (τ_i) and relative abundance (A_i) of each excited species, determined by the hydrostatic pressure-single photon counting method in degassed toluene solution at room temperature, measured in a high-pressure cell; λ_{ex} = 590 nm. [b] Not applicable.

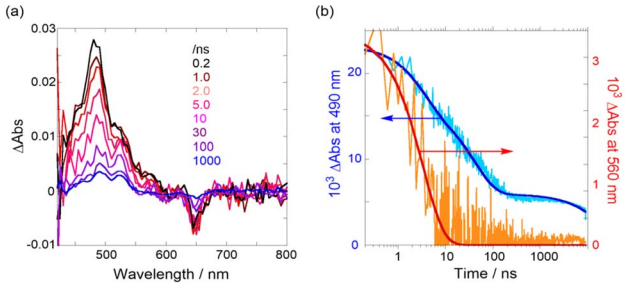

Fig. 6 (a) psTA spectra and (b) corresponding time profile of **Pc-CE-Pc** (64 μM) in degassed toluene at room temperature at 0.1 MPa. The measurements of psTA were performed by excitation source at 532 nm in a 2 mm cell.

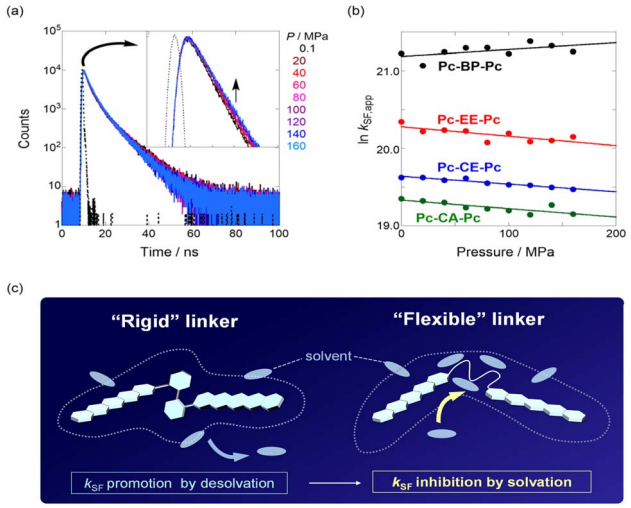

Fig. 7 (a) Pressure-dependent time-correlated fluorescence decays (λ_{ex} 590 nm, λ_{obs} 665 nm) of **Pc-CE-Pc** (41 μM) in toluene at 0.1, 20, 40, 60, 80, 100, 120, 140, and 160 MPa (from black to sky blue lines) at room temperature, measured in a high-pressure cell. The inset represents the enlarged figure. Also, the black dotted line shows the instrument response function. (b) Pressure dependence of apparent SF rate constants ($k_{SF,app}$) of **Pc-BP-Pc** (black, slope = 0.00089 ± 0.00051), **Pc-EE-Pc** (red, slope = −0.0012 ± 0.00038), **Pc-CE-Pc** (blue, slope = −0.0010 ± 0.00011), and **Pc-CA-Pc** (green, slope = −0.0011 ± 0.00029) in toluene at room temperature. (c) Conceptual scheme of total volumes in Pc dimers with "Rigid" *vs.* "Flexible" linkers.

fluorescence decay profiles of the present three Pc dimers were obviously of multiple components and reasonably fitted to a sum of two exponential functions to afford τ_1 and τ_2, respectively, in contrast to only the monoexponential function, τ_1, in the monomers. We adopted the biexponential fitting rather than the stretching fitting.[53] The previous paper[52] also concluded that the longer species is the monomer and shorter one is the SF component. These fluorescence lifetime data can be subjected to the eqn (1) for elucidating $k_{SF,app}$ for the new dimers; $k_{SF,app} = 6.84 \times 10^8$ s^{-1} for **Pc-EE-Pc**, 3.33×10^8 s^{-1} for **Pc-CE-Pc**, and 2.54×10^8 s^{-1} for **Pc-CA-Pc** in toluene at 0.1 MPa, as listed in Tables 1 and S13–S15. It should be noted that $k_{SF,app}$ obtained from the present eqn (1) is an apparent value because of the approximation based on the assumption that the reversed TTA process may be ignored due to the very slower reverse rather than the SF decay, according to our previous report.[22]

Before subjecting to the hydrostatic pressure-fluorescence lifetime measurements, we confirmed the reliability how to estimate $k_{SF,app}$ using the singlet excited-state fluorescence lifetimes. Therefore, we further measured picosecond transient absorption (psTA) spectrometry of **Pc-CE-Pc** as a representative dimer for the direct observation through TT and then T_1 from S_1 excitons. After excitation, a spectrum corresponding to singlet state was immediately observed, showing positive absorption bands from 450 to 600 nm (Fig. 6a). This spectrum gradually decayed, and after 100 ns, a different spectrum was observed with positive absorption bands in the 450–550 nm region and ΔAbs of zero in the 550–600 nm region. This spectrum corresponds to the triplet state. This trend in spectral shape is also in good agreement with previous reports using similar analogues.[45] The decay profile corresponding to only singlet state at 560 nm (Fig. 6b, red) can be reasonably fitted to one exponential function to give τ_s as 3.4 ns, and the decay at 490 nm corresponding to triplet state (Fig. 6b, blue) gave τ_{TT} as 43 ns and τ_T as 21 μs by fixing τ_s. The former decay (τ_s) from the singlet excited state indicates the nonradiative path from S_1 to TT, which is SF process, by the assumption as the negligible TTA mentioned above. The reciprocal fluorescence lifetime of τ_s should be treatable as $k_{SF,app} = 3.0 \times 10^8$ s^{-1}, which is almost same as the data obtained from the singlet fluorescence lifetimes (eqn (1)). This strongly reinforces the reliability of the estimation based on eqn (1), enabling us to elucidate the pressure-dependent $k_{SF,app}$ by the hydrostatic pressure-fluorescence lifetime measurements.

Thus, we measured pressure-dependent fluorescence lifetimes of the three Pc dimers and the corresponding reference monomers by the hydrostatic pressure time-correlated single-photon counting method. As shown in Fig. 7a, the fluorescence lifetime decay profiles of **Pc-CE-Pc** in toluene can be reasonably fitted to two exponential functions to afford τ_1 and τ_2, in contrast to the monotonic increasing of one excited-state species ($\tau_{1,ref}$) in **Pc-COO-^{i}Pr** with elevating hydrostatic pressure. According to eqn (1), the pressure-dependent $k_{SF,app}$ values in the three Pc dimers were obtained, the representative pressure

Table 2 Fluorescence lifetimes, apparent rate constants of singlet fission ($k_{SF,app}$), and activation volume changes ($\Delta V^{\ddagger}$) of the three Pc dimers in toluene under hydrostatic pressure[a]

Compd	P/MPa	τ_1/ns	A_1	τ_2/ns	A_2	χ^2	$k_{SF,app}/10^8$ s^{-1}	$\Delta V^{\ddagger}$/cm^3 mol^{-1}
Pc-EE-Pc (44 μM)	20	1.4	0.08	6.6	0.92	1.12	6.05	3.0 ± 0.9
	80	1.6	0.09	6.7	0.91	0.993	5.24	
	160	1.5	0.09	6.6	0.91	1.13	5.63	
Pc-CE-Pc (41 μM)	20	2.3	0.52	7.9	0.48	1.17	3.34	2.5 ± 0.3
	80	2.4	0.53	7.6	0.47	1.15	3.10	
	160	2.6	0.53	7.3	0.47	1.02	2.87	
Pc-CA-Pc (41 μM)	20	3.0	0.23	5.3	0.77	1.09	2.47	2.7 ± 0.7
	80	3.3	0.30	5.5	0.70	0.972	2.23	
	160	3.4	0.34	5.6	0.66	0.952	2.08	

[a] Fluorescence lifetime (τ_i) and relative abundance (A_i) of each excited species, determined by the hydrostatic pressure-single photon counting method in degassed toluene solution at room temperature, measured in a high-pressure cell; λ_{ex} = 590 nm.

Table 3 Solvent-dependent activation volume changes through iSF in the Pc dimers under hydrostatic pressure

Compd	$\Delta V^{\ddagger}$/cm^3 mol^{-1} in MCH	$\Delta V^{\ddagger}$/cm^3 mol^{-1} in toluene	$\Delta V^{\ddagger}$/cm^3 mol^{-1} in DCM
Pc-EE-Pc	6.8 ± 0.6	3.0 ± 0.9	1.9 ± 0.2
Pc-CE-Pc	3.7 ± 0.4	2.5 ± 0.3	−1.0 ± 0.4
Pc-CA-Pc	[a]	2.7 ± 0.7	[a]

[a] Not applicable due to the aggregation.

data of which are listed in Table 2 (all data are shown in Tables S2–S15). More importantly, these pressure-dependent kinetics allow us to further elucidate more quantitative SF dynamics upon hydrostatic pressurization, according to eqn (2):

$$\Delta V^{\ddagger} = -RT\left(\frac{\partial \ln\ k_{\mathrm{SF,app}}}{\partial P}\right) \quad (2)$$

As shown in Fig. 7b, the natural logarithm of $k_{\mathrm{SF,app}}$ was plotted as a function of pressure to give a slope as an activation volume change ($\Delta V^{\ddagger}$) in the transition state (TS) for the TT generation. We realized that on intercepts (0.1 MPa) in the plot, $k_{\mathrm{SF,app}}$ values ($\ln k_{\mathrm{SF,app}}$) of the three Pc dimers are smaller than that of previous **Pc-BP-Pc** (black line). This is likely ascribable to the linkers' flexibility, as revealed in Fig. 2. The important aspects are facts that the most flexible **Et** linker (red line) enables the faster TT formation rather than the relatively rigid **Cy** linker (blue and green lines). More interestingly, a gradual decreasing slope with increasing pressure was observed in each of the three PC dimers, corresponding to positive $\Delta V^{\ddagger}$ as 3.0 cm^3 mol^{-1} for **Pc-EE-Pc**, 2.5 cm^3 mol^{-1} for **Pc-CE-Pc**, and 2.7 cm^3 mol^{-1} for **Pc-CA-Pc**, in contrast to the negative $\Delta V^{\ddagger}$ (−2.5 cm^3 mol^{-1})[31] of **Pc-BP-Pc**. These results about positive $\Delta V^{\ddagger}$ in the present Pc dimers are highly likely to be explained in terms of spontaneous solvation that occurs around the polar functional groups in the TS, that is, expansion of total volume as illustrated in Fig. 7c, compared to the compactification based on the desolvation around the relatively non-polar biphenyl linker in **Pc-BP-Pc**. This solvation/desolvation scenario on the flexible polar linkers in the TS through SF may be corroborated by the facts about all the same degree as 2.5–3.0 cm^3 mol^{-1} in the three dimers. In other words, the degree of solvation may actively control iSF through the flexible polar linkers, which prompted us to further investigate the solvent effects of the three dimers under hydrostatic pressures.

Active switching of iSF under hydrostatic pressures

From the perspective of the operative mechanism proposed in the previous section, we performed solvent effects of the three Pc dimers, in which non-polar MCH and much polar dichloromethane (DCM), as compared to toluene, were employed. As **Pc-CA-Pc** in MCH induces the intermolecular J-aggregation that cannot estimate iSF as a monomeric **Pc-CA-Pc** species as mentioned above, **Pc-EE-Pc** and **Pc-CE-Pc** were subjected to the solvent-dependent iSF investigation upon hydrostatic pressurization. In a similar manner, for example, we measured the hydrostatic pressure-fluorescence lifetimes of the **Pc-EE-Pc** dimer and the corresponding **Pc-COO-^{i}Pr** monomer in MCH to give τ_2 and $\tau_{1,\mathrm{dimer}}$ for **Pc-EE-Pc** and $\tau_{1,\mathrm{ref}}$ for **Pc-COO-^{i}Pr**, respectively. The $\tau_{1,\mathrm{dimer}}$ and $\tau_{1,\mathrm{ref}}$ were subjected to the eqn (1) to afford all iSF data, listed in Table 3. As evident in Fig. 8a, only the data of **Pc-CE-Pc** in DCM provided the minus, inverted $\Delta V^{\ddagger}$ despite all the positive $\Delta V^{\ddagger}$. This indicates that the iSF suppression (solvation) is switchable to the iSF acceleration (desolvation) by changing from MCH and toluene to DCM under hydrostatic pressures; the data in **Pc-EE-Pc** are shown in Fig. S27. To more quantitatively confirm the hydrostatic pressure-responsive solvation inversion behavior, $E_{\mathrm{T}}(30)$[54] as an empirical polarity parameter determined by Reichardt's dye was used, as this parameter is based on the solvation around the large π-plane indicator: MCH (30.9 kcal mol^{-1}; using the value of cyclohexane because the Reichardt's dye is insoluble in MCH) < toluene (33.9 kcal mol^{-1}) < DCM (40.7 kcal mol^{-1}). As shown in Fig. 8b, the slopes of $\Delta V^{\ddagger}$–$E_{\mathrm{T}}(30)$ compensatory plot decrease with increasing $E_{\mathrm{T}}(30)$, which means that the degree of

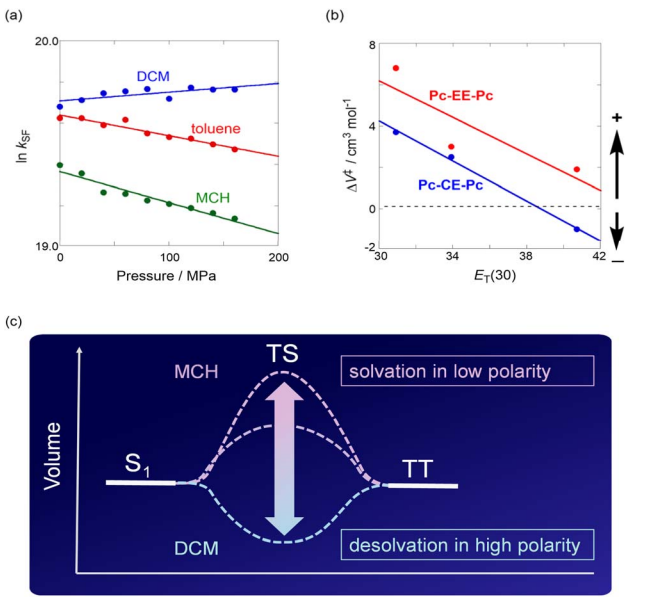

Fig. 8 (a) Pressure dependence of apparent SF rate constants ($k_{\mathrm{SF,app}}$) of **Pc-CE-Pc** in DCM (blue, r = 0.733, slope = 0.00042 ± 0.00015), toluene (red, r = 0.963, slope = −0.0010 ± 0.00011), and MCH (green, r = 0.965, slope = −0.0015 ± 0.00016). (b) The compensation plot of $\Delta V^{\ddagger}$–$E_{\mathrm{T}}(30)$ for **Pc-EE-Pc** (red, r = 0.864, slope = −0.44 ± 0.26) and **Pc-CE-Pc** (blue, r = 0.998, slope = −0.49 ± 0.027). (c) Volumetric diagram through iSF toward TT state.

solvation gradually weakened with increasing polarity. This can be attributed to the observation that the solvent molecules (DCM) having a higher degree of solvation may become repulsive around the excited carbonyl group in the Pc chromophore, resulting in the acceleration of iSF by desolvation of polar solvent molecules, as illustrated in Fig. 8c. It may be seen that both the straight lines (unit is omitted for simplicity) afford almost same slopes as −0.44 for **Pc-EE-Pc** and −0.49 for **Pc-CE-Pc**, respectively, indicating a single mechanism, that is (de) solvation on the flexible polar linkers, works and does not change in the solvent polarity range employed in each Pc dimer. Hence, the compactification upon hydrostatic pressurization is the main factor that governs not only acceleration but also switching of the degree of iSF on the flexible polar linkers, which was for the first time achievable under hydrostatic pressures. It should be therefore emphasized that such the compactification including the active switching of iSF cannot materialize at an ambient pressure (0.1 MPa).

Triplet exciton behavior through iSF under hydrostatic pressures

In this section, we investigate the behavior of the independent triplet excitons (T_1) formed through the iSF in the three Pc dimers under hydrostatic pressures, which allowed us to subject to the hydrostatic pressure-nanosecond transient absorption (nsTA) spectroscopic technique developed previously.[31] As shown in Fig. 9a, the representative spectra of **Pc-EE-Pc** in toluene showed an intense positive band around 400–550 nm that is assignable to an excited-state absorption (ESA) of T_1–T_n, which then decayed at microsecond intervals.[22,31] The pressure-dependent decays monitored at 495 nm (Fig. 9b) were found to gradually shorten, with increasing pressurization. Thus, the decays were reasonably fitted to a monoexponential function to afford the independent T_1 lifetimes (τ_T) from 12.2 μs at 0.1 MPa to 7.5 μs at 160 MPa in **Pc-EE-Pc** in toluene. This trend about the shortened τ_T was observed in other Pc dimers in toluene and MCH, which seems to be a general behavior of the independent T_1 excitons under hydrostatic pressures; all data are shown in Fig. S28–S31 (top panels) and Tables S16–S18. This can be ascribed to the fact that the excited T_1 excitons formed through the iSF are deactivated by pressure-induced higher viscosity of solvents, *e.g.*, 0.555 cP at 0.1 MPa to 1.508 cP at 160 MPa in toluene,[55] as was the case with **Pc-BP-Pc**. In general, τ_T was controlled by changing the solvent viscosity; τ_T in **Pc-BP-Pc** was prolonged from 0.36 μs in THF to 1.0 μs in THF/paraffin.[22] Thus, this discovery of the method to control τ_T only by changing hydrostatic pressure may further lead to a new controllable method of photosensitizing reactions through T_1, *e.g.*, the formation of $^1O_2$ in higher viscous biological environments.

In the previous section, we understood the factor that governs the iSF kinetics, which enables us to actively switch iSF processes upon hydrostatic pressurization. This provided us with in-depth mechanistic insights during the TT dissociation process (TT → $2T_1$). For this purpose, TT and T_1 quantum yields (Φ_{TT} and Φ_T) were estimated (see Materials and methods and Fig. S28–S31 (bottom panels)) and then the thermodynamic parameters were derived as $\Delta V^\circ_{TT\rightarrow T}$ in the equilibrium between TT and T_1, according to eqn (3):

$$\left(\frac{\partial \ln\left(\Phi_T/\Phi_{TT}\right)}{\partial P}\right) = -\frac{\Delta V^\circ_{TT\rightarrow T}}{RT} \quad (3)$$

As shown in Fig. 10a, the pressure-dependent Φ_T values in the three Pc dimers showed almost flat behavior with increasing hydrostatic pressure, in contrast to the distinct decreasing trend of **Pc-BP-Pc**. This difference can be easily described as follows: the biphenyl linker (**BP**) is known to cause the large structural change during the TT-T_1 process,[56] resulting in the distinct deactivation of Φ_T based on the pressure-induced changes of solvent properties. In contrast, it is highly likely that there are no restrictions for

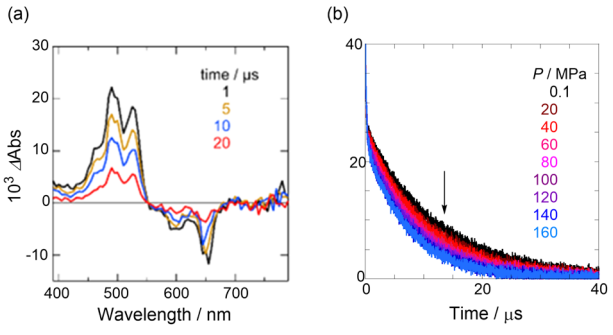

Fig. 9 (a) nsTA spectra of **Pc-EE-Pc** at 0.1 MPa and (b) corresponding decay profiles monitored at 495 nm in degassed toluene at 0.1, 20, 40, 60, 80, 100, 120, 140, and 160 MPa (from black to sky blue lines) at room temperature, measured in a high-pressure cell.

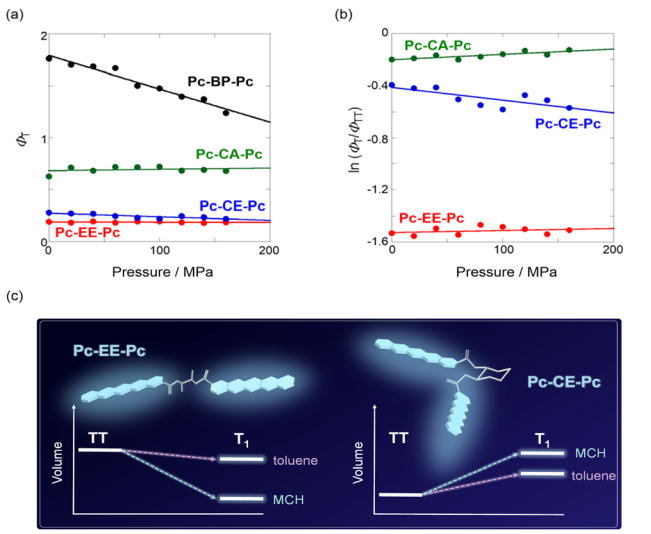

Fig. 10 Pressure dependence of (a) T_1 quantum yields (Φ_T) and (b) relative abundance ratios (Φ_T/Φ_{TT}) of **Pc-BP-Pc** (extracted from ref. 31 for comparison in only (a), $r = 0.979$, slope $= -0.0032 \pm 0.00025$), **Pc-EE-Pc** (red, $r = 0.222$, slope $= -2.1 \times 10^{-5} \pm 3.5 \times 10^{-5}$ (a) and $r = 0.287$, slope $= 0.00016 \pm 0.00020$ (b)), **Pc-CE-Pc** (blue, $r = 0.861$, slope $= -0.00035 \pm 7.8 \times 10^{-5}$ (a) and $r = 0.764$, slope $= -0.00099 \pm 0.00032$ (b)), and **Pc-CA-Pc** (green, $r = 0.240$, slope $= 0.00013 \pm 0.00020$ (a) and $r = 0.821$, slope $= 0.00041 \pm 0.00011$ (b)) in toluene at room temperature. (c) Volumetric diagram for the different formation of T_1 excitons in two Pc dimers.

Table 4 Solvent-dependent reaction volume changes through individual triplet generation in the Pc dimers under hydrostatic pressure

Compd	$\Delta V^{\circ}_{TT\rightarrow T}$ cm^{-3} mol^{-1} in toluene	$\Delta V^{\circ}_{TT\rightarrow T}$ cm^{-3} mol^{-1} in MCH
Pc-EE-Pc	-0.4 ± 0.5	-3.3 ± 1.0
Pc-CE-Pc	2.5 ± 0.8	6.3 ± 1.0
Pc-CA-Pc	-1.0 ± 0.3	[a]

[a] Not applicable due to the aggregation.

the present flexible linkers (**Cy** and **Et**) not only electronically but also sterically rather than **BP**, resulting in the no shifts of Φ_T during the T_1 formation under higher viscous environments upon hydrostatic pressurization. From this finding, it can be seen that the choice of linkers can overcome the drawbacks of the decreasing manner in Φ_T in response to hydrostatic pressure stimulation. Furthermore, from the analysis by eqn (3), it can be seen that $\Delta V^{\circ}_{TT\rightarrow T}$ values were inverted from -0.4 cm^3 mol^{-1} for **Pc-EE-Pc** to 2.5 cm^3 mol^{-1} for **Pc-CE-Pc**, as shown in Fig. 10b and Table 4. This behavior can also be explained by solvation/desolvation effect: during the T_1 formation, on the more flexible linker **Et**, solvated solvent molecules are considered to be easily released (desolvation = negative ΔV°). In contrast, solvation molecules in the slightly congested **Cy** linker may easily be trapped (solvation = positive ΔV°), as illustrated in Fig. 10c. It is therefore noteworthy that even the difference in the flexible linkers can control the degree of the T_1 formation by hydrostatic pressure, which indicates that this is "critical molecular design" that enables us to control iSF (active switching), τ_T (shortened), Φ_T (no decreasing), and T_1 formation (also active switching).

Conclusions

In this study, we investigated how and to what extent flexible linkers between the SF-active chromophores, Pc, affects the SF process and the independent T_1 formation using hydrostatic pressure as an external stimulation. The comprehensive studies under ambient and high pressures revealed that the flexibility of the linkers plays decisive roles in controlling the iSF dynamics and T_1 thermodynamics, and has the capability to actively switch both of them. As a new additional discovery on the hydrostatic pressure SF chemistry, the shortened T_1 lifetime and non-decreasing T_1 quantum yield are features of unique excitons. This opens a new avenue for the hydrostatic pressure-controlled photosensitizing reactions. In detail, the choice of linkers and polar groups type in the dimer skeleton gave us more flexibility in molecular design. This study provides guidelines for critical molecular design that can actively control SF and its related photophysics/photochemistry in response to hydrostatic pressure, facilitating the development of advanced piezo-sensitive soft materials.

Materials and methods

Materials

All commercially available reagents and solvents were used as received. Spectroscopic-grade toluene, MCH, and DCM were used as solvents without further purification. The synthesis and characterization of the new compounds used in this study are shown in S50–S59 in SI.

Instruments

Melting points were measured with a Büchi M-560 apparatus. HR-MS spectra were obtained by using a Bruker ESI micrOTOF II. ^{1}H (400 MHz) and ^{13}C NMR spectra (100 MHz) were recorded using a JEOL ECX-400 spectrometer. ^{1}H (500 MHz) and ^{13}C NMR spectra (125 MHz) were recorded using a JEOL ECX-500 spectrometer. UV/vis spectra were measured in a high-pressure cell using a JASCO V-650. Fluorescence spectra were measured in a high-pressure cell by using a JASCO FP-8500. Fluorescence lifetime decays were measured in a high-pressure cell by using a Hamamatsu Quantaurus-Tau single-photon counting apparatus fitted with an LED light source. CD spectra were measured in a high-pressure cell by using a JASCO J-720WI. nsTA spectra were recorded using a laser flash photolysis system with a time resolution (IRF) of *ca.* 20 ns (FWHM). Excitation was performed at 532 nm. And, nsTA spectra were obtained by using a Unisoku TSP-2000 flash spectrometer–pump pulse source: Surelite-I Nd:YAG (Continuum, 4–6 ns fwhm) laser with the second harmonic at 532 nm, monitor light source: xenon lamp (150 W), and detector: photomultiplier tube. Picosecond transient absorption measurements were performed using the UNISOK instrument using the randomly interleaved pulse train method[57] with a time resolution (IRF) of *ca.* 20 ps (FWHM). Excitation was performed at 532 nm.

Hydrostatic pressure spectroscopy

UV/vis and fluorescence spectroscopy and fluorescence lifetime and nsTA measurements under hydrostatic pressures were performed using a custom-built high-pressure apparatus.[31,37] The method is summarized as follows. The sample solution was sealed in a quartz inner cell (2 mm path length), and then the cell was set into the outer cell with sapphire windows. The outer cell was hydrostatically pressurized by water and then placed in the optical systems (see Fig. S1).

Determination of TT (Φ_{TT}) and T_1 quantum yields (Φ_T) of Pc dimers (PcD)

Each quantum yield under hydrostatic pressures was elucidated by the similar method that can consistently be established in the previous report.[31] Thus, Φ_{TT} was estimated using eqn (4):

$$\frac{k_{SF,app}}{k_0 + k_{SF,app}} = \Phi_{TT} \quad (4)$$

where pressure-dependent k_0 and $k_{SF,app}$ are specified in Tables S9–S15.

$\Phi_{T,PcD}$ values were calculated in relation to that of zinc tetraphenylporphyrin (ZnTPP, $\Phi_{T,ZnTTP}$), using eqn (5):

$$\Phi_{T,PcD} = \frac{\Delta A_{T,\,PcD}}{\Delta A_{T,ZnTPP}} \times \frac{\varepsilon_{T,\,ZnTTP}}{\varepsilon_{T,\,PcD}} \times \frac{Abs_{ZnTPP}}{Abs_{PcD}} \times \Phi_{T,\,ZnTTP} \quad (5)$$

for example, in the case of **Pc-EE-Pc** at 20 MPa:

$$= \frac{0.025}{0.117} \times \frac{73000}{78000} \times \frac{0.070}{0.068} \times 0.88 = 0.182$$

where ε_T, ΔA, and Abs denote the excitation coefficient at T_1 state, delta absorbance in nsTA, and absorbance at 532 nm in the steady-state absorption measurements, respectively. ΔA_{ZnTPP} ($\Delta A_{ZnTPP} = 0.117$ in toluene, 470 nm, 20 MPa) was observed at 470 nm and ΔA_{PcD} ($\Delta A_{\mathbf{Pc\text{-}EE\text{-}Pc}} = 0.025$ in toluene, 495 nm, 20 MPa) was observed at T_1 spectral peak top (EE, CE: 495 nm, CA: 520 nm). $\Phi_{T,ZnTTP}$ and $\varepsilon_{T,ZnTTP}$ were acquired from a previous study[58] ($\lambda_{ex} = 530$ nm, $\lambda_{obs} = 470$ nm in toluene; $\Phi_{T,ZnTTP} = 0.88$, $\varepsilon_{T,ZnTTP} = 73\,000\ M^{-1}\ cm^{-1}$). Data of Abs. (532 nm,PcD) are shown in Fig. S9–S11 ($Abs_{ZnTPP} = 0.070$, $Abs_{\mathbf{Pc\text{-}EE\text{-}Pc}} = 0.068$ at 20 MPa). $\varepsilon_{T,PcD}$ was calculated using eqn (6)–(8):

$$\frac{\tau_0}{\tau} = 1 + k_{EnT}\tau_0[PcD] \quad (6)$$

$$\Phi_{EnT} = \frac{k_{EnT}[PcD]}{k_{EnT}[PcD] + k_{Anth}} \quad (7)$$

$$\varepsilon_{T,\,PcD} = \varepsilon_{T,\,anth} \frac{\Delta Abs_{PcD}}{\Delta Abs_{Anth}} \frac{1}{\Phi_{EnT}} \quad (8)$$

As a result, $\varepsilon_{T,\mathbf{Pc\text{-}EE\text{-}Pc}} = 78\,000\ M^{-1}\ cm^{-1}$ at 495 nm, $\varepsilon_{T,\mathbf{Pc\text{-}EE\text{-}Pc}} = 91\,000\ M^{-1}\ cm^{-1}$ at 495 nm, and $\varepsilon_{T,\mathbf{Pc\text{-}EE\text{-}Pc}} = 55\,000\ M^{-1}\ cm^{-1}$, respectively (All data were measured in toluene). For details, see Fig. S32–S34 and ref. 22.

Author contributions

G. F. initiated and supervised the whole study. G. F. and T. H. designed the project and the experiments. R. O., T. K. and T. K. performed the spectroscopic experiments. H. S. and M. H. designed and performed the transient absorption spectroscopic experiments. All authors contributed to writing the manuscript.

Conflicts of interest

There are no conflicts to declare.

Data availability

The data supporting this article have been uploaded as part of the supporting information (SI). Supplementary information is available. See DOI: **https://doi.org/10.1039/d5sc04791a**.

Acknowledgements

This work was supported by Grants-in-Aid (no. JP23K04708 to H.S., No. JP23H04876 and JP24K01473 to T.H., and no. JP23H04020, JP24K01536, and JP24K21791 to G.F.) from the Japan Society for the Promotion of Science (JSPS), IZUMI SCIENCE AND THCHNOLOGY FOUNDATION (to G.F.), and Ajinomoto Co., Inc. (to G.F.).

References

1 F. Auzel, *Chem. Rev.*, 2004, **104**, 139–173.
2 J. Zhou, Q. Liu, W. Feng, Y. Sun and F. Li, *Chem. Rev.*, 2015, **115**, 395–465.
3 N. Yanai and N. Kimizuka, *Acc. Chem. Res.*, 2017, **50**, 2487–2495.
4 M. B. Smith and J. Michl, *Chem. Rev.*, 2010, **110**, 6891–6936.
5 K. Miyata, F. S. Conrad-Burton, F. L. Geyer and X.-Y. Zhu, *Chem. Rev.*, 2019, **119**, 4261–4292.
6 T. Ullrich, D. Munz and D. M. Guldi, *Chem. Soc. Rev.*, 2021, **50**, 3485–3518.
7 B. J. Walker, A. J. Musser, D. Beljonne and R. H. Friend, *Nat. Chem.*, 2013, **5**, 1019–1024.
8 M. J. Y. Tayebjee, S. N. Sanders, E. Kumarasamy, L. M. Campos, M. Y. Sfeir and D. R. McCamey, *Nat. Phys.*, 2017, **13**, 182–189.
9 J. Zirzlmeier, D. Lehnherr, P. B. Coto, E. T. Chernick, R. Casillas, B. S. Basel, M. Thoss, R. R. Tykwinski and D. M. Guldi, *Proc. Natl. Acad. Sci. U. S.*, 2015, **112**, 5325–5330.
10 N. V. Korovina, C. H. Chang and J. C. Johnson, *Nat. Chem.*, 2020, **12**, 391–399.
11 M. Majdecki, C.-H. Hsu, C.-H. Wang, E. H.-C. Shi, M. Zakrocka, Y.-C. Wei, B.-H. Chen, C.-H. Lu, S.-D. Yang, P.-T. Chou and P. Gaweł, *Angew. Chem., Int. Ed.*, 2024, **63**, e202401103.
12 T. Tsuneda and T. Taketsugu, *Sci. Rep.*, 2024, **14**, 829.
13 T. Saegusa, H. Sakai, H. Nagashima, Y. Kobori, N. V. Tkachenko and T. Hasobe, *J. Am. Chem. Soc.*, 2019, **141**, 14720–14727.
14 D. Chen, J. Shao, T. Zhang, K. Xu, C. Liang, Y. Cai, Y. Guo, P. Chen, X.-Z. Mou and X. Dong, *Nano Lett.*, 2024, **24**, 7524–7533.
15 Y. Liu, J. Li, S. Gong, Y. Yu, Z.-H. Zhu, C. Ji, Z. Zhao, X. Chen, G. Feng and B. Z. Tang, *ACS Materials Lett.*, 2024, **6**, 896–907.
16 W.-L. Chan, T. C. Berkelbach, M. R. Provorse, N. R. Monahan, J. R. Tritsch, M. S. Hybertsen, D. R. Reichman, J. Gao and X.-Y. Zhu, *Acc. Chem. Res.*, 2013, **46**, 1321–1329.
17 D. Casanova, *Chem. Rev.*, 2018, **118**, 7164–7207.
18 J. J. Burdett, D. Gosztola and C. J. Bardeen, *J. Chem. Phys.*, 2011, **135**, 214508.
19 M. W. B. Wilson, A. Rao, K. Johnson, S. Gélinas, R. di Pietro, J. Clark and R. H. Friend, *J. Am. Chem. Soc.*, 2013, **135**, 16680–16688.
20 S. Nakamura, H. Sakai, M. Fuki, Y. Kobori, N. V. Tkachenko and T. Hasobe, *J. Phys. Chem. Lett.*, 2021, **12**, 6457–6463.

21 X. Zhao, J. P. O'Connor, J. D. Schultz, Y. J. Bae, C. Lin, R. M. Young and M. R. Wasielewski, *J. Phys. Chem. B*, 2021, **125**, 6945–6954.
22 T. Sakuma, H. Sakai, Y. Araki, T. Mori, T. Wada, N. V. Tkachenko and T. Hasobe, *J. Phys. Chem. A*, 2016, **120**, 1867–1875.
23 A. M. Alvertis, S. Lukman, T. J. H. Hele, E. G. Fuemmeler, J. Feng, J. Wu, N. C. Greenham, A. W. Chin and A. J. Musser, *J. Am. Chem. Soc.*, 2019, **141**, 17558–17570.
24 A. Aster, F. Zinna, C. Rumble, J. Lacour and E. Vauthey, *J. Am. Chem. Soc.*, 2021, **143**, 2361–2371.
25 A. J. Tilley, R. D. Pensack, E. L. Kynaston, G. D. Scholes and D. S. Seferos, *Chem. Mater.*, 2018, **30**, 4409–4421.
26 L. Catti, H. Narita, Y. Tanaka, H. Sakai, T. Hasobe, N. V. Tkachenko and M. Yoshizawa, *J. Am. Chem. Soc.*, 2021, **143**, 9361–9367.
27 G. Lavarda, A. Sharma, M. Beslać, S. A. H. Jansen, S. C. J. Meskers, R. H. Friend, A. Rao and E. W. Meijer, *J. Am. Chem. Soc.*, 2024, **146**, 28985–28993.
28 M. Fukumitsu, T. Fukui, Y. Shoji, T. Kajitani, R. Khan, N. V. Tkachenko, H. Sakai, T. Hasobe and T. Fukushima, *Sci. Adv.*, 2024, **10**, eadn7763.
29 G. S. Doucette, H.-T. Huang, J. M. Munro, K. T. Munson, C. Park, J. E. Anthony, T. Strobel, I. Dabo, J. V. Badding and J. B. Asbury, *Cell Rep. Phys. Sci.*, 2020, **1**, 100005.
30 Y. Huang, Q. Gong, J. Ge, P. Tang, F. Yu, L. Xiao, Z. Wang, H. Sun, J. Yu, D.-S. Li, Q. Xiong and Q. Zhang, *ACS Nano*, 2020, **14**, 15962–15972.
31 T. Kinoshita, S. Nakamura, M. Harada, T. Hasobe and G. Fukuhara, *Chem. Sci.*, 2023, **14**, 3293–3301.
32 L. Wang, R. Zhu, R. Pu, W. Liu, Y. Lu and T.-C. Weng, *Nanomaterials*, 2024, **14**, 1487.
33 C. Hetz, *Nat. Rev. Mol. Cell Biol.*, 2012, **13**, 89–102.
34 K. Matsumoto, K. Nakagawa, D. Asanuma and G. Fukuhara, *Front. Chem.*, 2024, **12**, 1478034.
35 A. Drljaca, C. D. Hubbard, R. van Eldik, T. Asano, M. V. Basilevsky and W. J. le Noble, *Chem. Rev.*, 1998, **98**, 2167–2289.
36 J. L. Silva, A. C. Oliveira, T. C. R. G. Vieira, G. A. P. de Oliveira, M. C. Suarez and D. Foguel, *Chem. Rev.*, 2014, **114**, 7239–7267.
37 H. Mizuno and G. Fukuhara, *Acc. Chem. Res.*, 2022, **55**, 1748–1762.
38 F. A. Bovey and S. S. Yanari, *Nature*, 1960, **186**, 1042–1044.
39 P. C. Johnson and H. W. Offen, *J. Chem. Phys.*, 1972, **56**, 1638–1642.
40 K. Hara and K. Obara, *Chem. Phys. Lett.*, 1985, **117**, 96–98.
41 K. Hara, T. Arase and J. Osugi, *J. Am. Chem. Soc.*, 1984, **106**, 1968–1972.
42 K. Hara, H. Suzuki and W. Rettig, *Chem. Phys. Lett.*, 1988, **145**, 269–272.
43 C. Yang, T. Mori, Y. Origane, Y. H. Ko, N. Selvapalam, K. Kim and Y. Inoue, *J. Am. Chem. Soc.*, 2008, **130**, 8574–8575.
44 A. J.-L. Ayitou, G. Fukuhara, E. Kumarasamy, Y. Inoue and J. Sivaguru, *Chem. Eur. J.*, 2013, **19**, 4327–4334.
45 H. Sakai, R. Inaya, H. Nagashima, S. Nakamura, Y. Kobori, N. V. Tkachenko and T. Hasobe, *J. Phys. Chem. Lett.*, 2018, **9**, 3354–3360.
46 H. Bian, L. Ye, W. Zhong and J. Sun, *Tetrahedron*, 2019, **75**, 449–457.
47 N. J. Hestand and F. C. Spano, *Chem. Rev.*, 2018, **118**, 7069–7163.
48 H. Mizuno, M. Kitamatsu, Y. Imai and G. Fukuhara, *ChemPhotoChem*, 2020, **4**, 502–507.
49 T. Kinoshita, Y. Imai and G. Fukuhara, *J. Phys. Chem. B*, 2021, **125**, 5952–5958.
50 T. Kinoshita, K. Fujise, E. Tsurumaki, S. Toyota and G. Fukuhara, *Chem. Commun.*, 2022, **58**, 3290–3293.
51 N. Berova, L. D. Bari and G. Pescitelli, *Chem. Soc. Rev.*, 2007, **36**, 914–931.
52 S. Lukman, K. Chen, J. M. Hodgkiss, D. H. P. Turban, N. D. M. Hine, S. Dong, J. Wu, N. C. Greenham and A. J. Musser, *Nat. Commun.*, 2016, **7**, 13622.
53 W. Kim, N. A. Panjwani, K. C. Krishnapriya, K. Majumder, J. Dasgupta, R. Bittl, S. Patil and A. J. Musser, *Cell. Rep. Phys. Sci.*, 2024, **5**, 102045.
54 C. Reichardt, *Chem. Rev.*, 1994, **94**, 2319–2358.
55 M. J. Assael, H. M. T. Avelino, N. K. Dalaouti, J. M. N. A. Fareleira and K. R. Harris, *Int. J. Thermophys.*, 2001, **22**, 789–799.
56 Y. Kobori, M. Fukui, S. Nakamura and T. Hasobe, *J. Phys. Chem. B*, 2020, **124**, 9411–9419.
57 T. Nakagawa, K. Okamoto, H. Hanada and R. Katoh, *Opt. Lett.*, 2016, **41**, 1498–1501.
58 T. H. Tran-Thi, C. Desforge, C. Thiec and S. Gaspard, *J. Phys. Chem.*, 1989, **93**, 1226–1233.